

# Proceedings of the Institution of Mechanical Engineers, Part J: Journal of Engineering Tribology

<http://pij.sagepub.com/>

---

## **Elastohydrodynamic modelling of heat partition in rolling-sliding point contacts**

A Clarke, K. J. Sharif, H. P. Evans and R. W. Snidle

*Proceedings of the Institution of Mechanical Engineers, Part J: Journal of Engineering Tribology* 2007 221: 223

DOI: 10.1243/13506501JET219

The online version of this article can be found at:

<http://pij.sagepub.com/content/221/3/223>

---

Published by:



<http://www.sagepublications.com>

On behalf of:



[Institution of Mechanical Engineers](http://www.institutionofmechanicalengineers.org)

Additional services and information for *Proceedings of the Institution of Mechanical Engineers, Part J: Journal of Engineering Tribology* can be found at:

**Email Alerts:** <http://pij.sagepub.com/cgi/alerts>

**Subscriptions:** <http://pij.sagepub.com/subscriptions>

**Reprints:** <http://www.sagepub.com/journalsReprints.nav>

**Permissions:** <http://www.sagepub.com/journalsPermissions.nav>

**Citations:** <http://pij.sagepub.com/content/221/3/223.refs.html>

>> [Version of Record](#) - Mar 1, 2007

[What is This?](#)

# Elastohydrodynamic modelling of heat partition in rolling–sliding point contacts

A Clarke\*, K J Sharif, H P Evans, and R W Snidle

Cardiff School of Engineering, Cardiff University, Cardiff, UK

*The manuscript was received on 26 July 2006 and was accepted after revision for publication on 23 January 2007.*

DOI: 10.1243/13506501JET219

**Abstract:** This article presents the results of a series of thermal elastohydrodynamic lubrication (EHL) analyses of a set of disc experiments carried out by Patching *et al.* The authors have previously calculated the heat partition at each load stage from the experimental data, and the present work seeks to compare the heat partition developed in a thermal EHL analysis of the lubricant film with that calculated from the experiments. These EHL analyses show that the heat partition depends on the non-Newtonian formulation used. Only when the dissipation takes place by wall slip occurring at the faster moving surface do the heat partition results approach those determined from the experimental results. It is concluded that this combination of experimental heat partition results with associated EHL analysis can prove to be a much more discerning test of rheological behaviour in EHL contacts than is provided by measurement of traction.

**Keywords:** traction, flash temperatures, heat partition, non-Newtonian, thermal elastohydrodynamic lubrication, limiting shear stress

## 1 INTRODUCTION

In the study of elastohydrodynamic lubrication (EHL), thermal behaviour of the oil film is of great interest. The way in which heat is developed within, and dissipated from, the oil film, can greatly affect the temperatures developed on the surfaces of the contacting solid bodies. It is this fundamental issue of how the lubricant rheology affects the way in which heat is generated within the oil film, and in turn how that affects the partition of heat between the solid surfaces, which is the subject of this article.

Blok [1, 2] and subsequent works by Tian and Kennedy [3] and Bos and Moes [4] have developed widely used methods for the calculation of flash temperatures and heat partition in dry contact. However, their approaches are not strictly appropriate when lubricated contacts are considered. Fluid film

lubrication of heavily loaded concentrated contacts is achieved by means of EHL where the pressures developed in the lubricant lead to significant increase in viscosity together with elastic deflection of the surfaces. When sliding of the surfaces occurs, heat is generated within the film by shearing and compressive heating of the lubricant. The dominant heat transfer mechanism is that of conduction perpendicular to the film. If heat is generated throughout the thickness of the film, the highest temperatures are developed within the film itself, and the temperature gradient necessary to transport the heat by conduction to the surfaces ensures that the surfaces are at lower and generally different temperatures. Thus, the lubricant film must be considered in any study of thermal behaviour of lubricated contacts.

Manton *et al.* [5] developed a numerical temperature model for heavily loaded line contacts, which considers the lubricant film. Their analysis was based on an assumed Hertzian semi-elliptical pressure distribution and a film thickness based on the well-known Dowson and Higginson formula, rather than a full EHL analysis. Their analysis uses the surface bulk (skin) temperatures as inlet boundary conditions and

\*Corresponding author: Cardiff School of Engineering, Cardiff University, Queen's Buildings, The Parade, Newport Road, Cardiff CF24 3AA, UK. email: [clarkeA7@cf.ac.uk](mailto:clarkeA7@cf.ac.uk)

assumes that these are known or can be estimated and then calculates contact temperatures and the heat partition.

The development of more sophisticated numerical analyses of the EHL problem in the intervening period has allowed detailed thermal EHL models to be developed, which remove the need for simplifying assumptions. Cheng [6] was one of the first researchers to produce a numerical solution to the thermal EHL problem. However, the load was extremely low and, hence, the influence of thermal effects on film shape and thickness was insignificant. Sui and Sadeghi [7, 8] developed a modified Reynolds equation to incorporate Eyring-type non-Newtonian rheology. They solved the Reynolds and elastic equations using the Newton–Raphson technique and adopted a finite-element formulation for the energy equation. They used their model to compare isothermal and thermal non-Newtonian traction behaviours, under different amounts of sliding.

The thermal non-Newtonian model of Yang and Wen [9] compared five different rheological models in an investigation of the effects of non-Newtonian and thermal behaviour on line contacts. Hsiao and Hamrock [10] also developed a thermal line-contact model and used it to analyse the temperature distributions within the lubricant film over a wide range of sliding conditions, from pure rolling to opposite sliding, in an investigation of lubricant degradation under high temperatures.

Wolff *et al.* [11] developed a thermal Newtonian line-contact model, which solved the Reynolds, film thickness, and energy equations using an approach similar to that of Sui and Sadeghi. They investigated the effect of various viscosity models on calculated traction coefficient.

Recent work has seen the thermal non-Newtonian EHL models extended to cover the analysis of worm gears [12], variable ratio transmissions [13], starved contacts [14], rough surfaces [15], and mixed lubrication conditions [16].

The authors have previously studied experimental results from disc machine tests [17] and calculated the heat partition using a heat transfer model, which considered the temperatures developed within the discs and shafts. The work reported here uses a thermal EHL model applied to the contact between the experimental discs (with inlet temperature boundary conditions specified from the previously reported heat transfer model) to investigate the effects of various non-Newtonian rheological models and viscosity–pressure–temperature models on the heat generation within the oil film and the heat partition between the surfaces, in an attempt to further understand the heat partition behaviour determined from the experimental results.

## 2 EXPERIMENTAL WORK AND HEAT TRANSFER MODELS

The experimental work modelled in this article used a recirculating power, high-speed two-disc machine, to investigate the scuffing failure of ground and super-finished discs under conditions typically found in gas turbine gearing [18]. The discs were 76.2 mm in diameter and crowned to give an elliptical Hertzian contact, with an aspect ratio of 1:4, with its major axis parallel to the axis of the discs.

The discs were mounted on parallel shafts, which were gear connected to recirculate the power transmitted at the rolling/sliding contact and to give a fixed slide/roll ratio. The faster shaft was mounted on fixed bearings, whereas the slower shaft was mounted on bearings carried by a swinging yoke, through which load could be applied to the contact by means of a hydraulic ram.

Thermocouples were embedded in the test discs, 3.2 mm below the disc surface at the centre-line of the running track and a torque dynamometer was mounted on the drive shaft of the slow disc and was used to measure the torque developed in the shaft continuously and thus the friction at the disc contact. This torque was due to both the frictional traction due to sliding between the discs and that due to the friction of the bearings in which the slow shaft was mounted. The bearing friction was carefully measured in the test rig as a function of load and speed, in a calibration under pure rolling conditions. The temperature and friction measurements were recorded continuously.

The test discs were spray-lubricated using a constant flowrate jet directed at the contact. The lubricant used was Mobil Jet 2, a synthetic gas turbine oil, which was circulated to the test head at a controlled temperature of 100 °C.

Full details of the disc machine and the scuffing experiments are given by Patching *et al.* [18]. During the tests, the discs were run at a constant speed. At the start of each test, oil was circulated through the test head and the discs run together at a very light load until the temperatures stabilized. The first load was then applied, corresponding to a maximum Hertzian contact pressure  $p_o = 0.6$  GPa, and held constant for 3 min. The load was increased, to give  $p_o = 0.7$  GPa, and held constant for a further 3 min. This procedure was repeated in steps of 0.1 GPa at 3 min intervals, until the discs scuffed or the maximum load was reached, corresponding to  $p_o = 1.7$  GPa. A typical trace of recorded temperatures and friction force corresponding to Patching's experiment 2-13 can be seen in Fig. 1.

The authors subsequently developed a heat conduction model of the disc and shaft assemblies, in

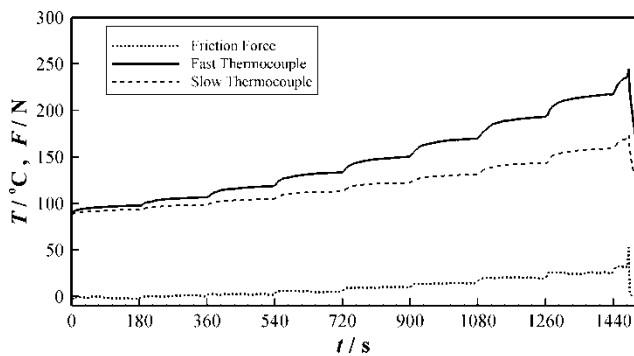


Fig. 1 Test trace of test 2-13

order to predict temperatures within the fast and slow discs and to investigate the way in which heat is partitioned between the surfaces. A full explanation of the conduction model may be found in Clarke *et al.* [17], but a brief description of the model and its results are given here.

A two-dimensional transient conduction model was developed, which calculated the average temperatures in the generating cross-section of the disc and shaft, neglecting any circumferential variation. It used the frictional heat generated at the contact as an input and also included the convective heat losses from the disc and shaft surfaces to the air-oil spray mixture circulating in the test head. The total frictional heat measured in the experiment was partitioned between the surfaces by a factor,  $\beta$ , where  $0 \leq \beta \leq 1$  and represents the fraction of the total heat that passes into the faster disc. The remaining fraction  $(1 - \beta)$  was assumed to pass into the slower disc. The heat input to each disc was then distributed according to the Hertzian pressure distribution. Factor  $\beta$  was adjusted until the calculated temperatures at the position of the thermocouple matched those recorded in the experiment.  $\beta$  was assumed to remain constant over each 3 min load stage, but was allowed to differ between load stages in the same experiment. The heat transfer coefficients for the various surfaces were estimated from reference expressions for rotating plane and cylindrical surfaces and adjusted as described in reference [17] to ensure that the overall test disc temperature balance was maintained.

Nine different tests were modelled in this way, five of which used ground discs with the remainder using super-finished discs, details of which may be found in reference [17]. Figure 2 gives the calculated temperature trace for test 2-13, showing excellent agreement with the experimental result of Fig. 1. The figure shows the calculated temperatures at the thermocouple position and also on the centre-line of the running track, for both slow and fast discs. The friction trace shown in Fig. 2 differs from that shown in

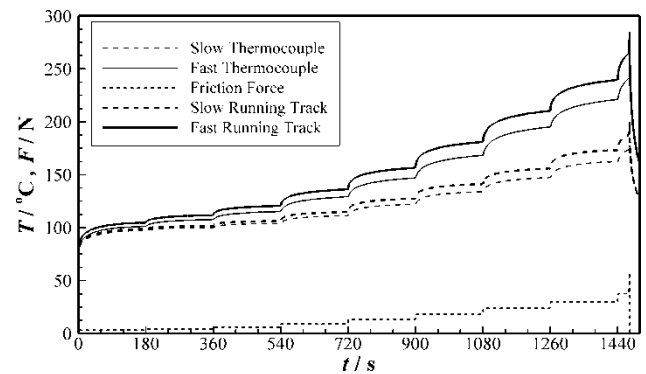


Fig. 2 Calculated temperatures from two-dimensional transient model for test 2-13

Fig. 1 because of the adjustment made to eliminate bearing friction.

It was found that the heat partition required to match the temperatures of the model and the experimental results strongly favoured the faster disc, with values of  $\beta$  between 0.75 at lower load stages and 0.6 at the higher load stages. It was found that  $\beta$  was related to the product of the sliding speed and the surface temperature difference between fast and slow discs. This trend can be seen in Fig. 3, where each data point represents the value of  $\beta$  required to match the temperatures over a particular load stage.

It can be seen from Fig. 2 that at the end of each load stage, the temperatures reach an approximately steady-state, and it is these conditions to which the thermal EHL solver is applied in the work reported here.

The results from the two-dimensional conduction model are used to provide inlet temperature boundary conditions for the thermal EHL models. Three-dimensional analyses of the discs reported in reference [17] confirm that these are the appropriate

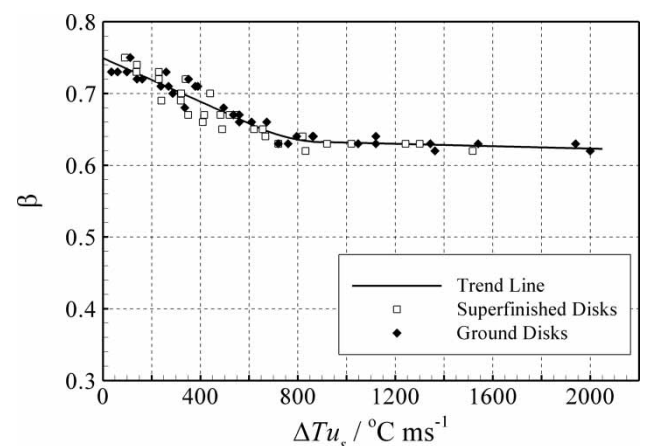


Fig. 3 Variation of heat partition parameter with product of surface temperature difference between discs and sliding velocity

boundary conditions. Temperature boundary conditions are often a source of uncertainty in thermal EHL work, but are known here with some confidence from the conduction modelling.

### 3 EHL MODELLING

#### 3.1 Governing equations

The point contact thermal EHL model used in this work is essentially that described by Sharif *et al.* [12, 13], but it is outlined here for completeness. The analysis includes both shear heating and compressive heating/cooling in its formulation, together with convective heat transfer within the oil film.

Reynolds equation (1) describes the hydrodynamic aspects of the steady-state EHL mechanism, where sliding and entrainment are in the  $x$  direction only

$$\frac{\partial}{\partial x} \left\{ \sigma_x \frac{\partial p}{\partial x} \right\} + \frac{\partial}{\partial y} \left\{ \sigma_y \frac{\partial p}{\partial y} \right\} = \frac{\partial}{\partial x} (\rho \hat{u} h) \quad (1)$$

The flow factors,  $\sigma_x$  and  $\sigma_y$ , are obtained from the appropriate non-Newtonian rheological model, as described in detail in reference [12].

The elastic deflection is given using the deflection of semi-infinite bodies, such that the film thickness is given by equation (2)

$$h(x, y) = h_0 + \frac{x^2 + y^2}{2R} + \frac{2}{\pi E'} \iint_A \frac{p(x', y')}{\sqrt{(x' - x)^2 + (y' - y)^2}} dx' dy' \quad (2)$$

In the solution scheme, the deflection equation takes the differential form developed by Holmes *et al.* [19], such that the equation is discretized as

$$\frac{\partial^2 h(x_i, y_j)}{\partial x^2} + \frac{\partial^2 h(x_i, y_j)}{\partial y^2} = \frac{2}{R} + \frac{2}{\pi E'} \sum_{\text{all } k, l} f_{k-i, l-j} p_{k, l} \quad (3)$$

where  $f_{i, j}$  are the weighting functions for the influence of pressure on the deflection Laplacian and are evaluated as described in reference [20]. These weighting functions decay rapidly with increasing index, thus allowing equations (1) and (3) to be solved as a coupled pair, as described in reference [19].

The energy equation for the fluid is given by

$$\begin{aligned} & \rho c \left( u \frac{\partial \theta}{\partial x} + v \frac{\partial \theta}{\partial y} \right) \\ &= \tau_x \frac{\partial u}{\partial z} + \tau_y \frac{\partial v}{\partial z} + \varepsilon \theta \left( u \frac{\partial p}{\partial x} + v \frac{\partial p}{\partial y} \right) \\ &+ \frac{\partial}{\partial x} \left( k \frac{\partial \theta}{\partial x} \right) + \frac{\partial}{\partial y} \left( k \frac{\partial \theta}{\partial y} \right) + k \left( \frac{\partial^2 \theta}{\partial z^2} \right) \end{aligned} \quad (4)$$

and surface temperatures of the contacting solids, which form the boundary conditions for equation (4), are obtained using a one-dimensional (linear heat flow) conduction model of the form

$$\theta_s = \theta_B + \frac{1}{\sqrt{\pi k \rho c}} \int_0^t \frac{q \, d\lambda}{\sqrt{t - \lambda}} \quad (5)$$

where  $\theta_s(x, y)$  is the surface temperature of the solid and  $\theta_B$  is that at the inlet boundary. The integration in equation (5) is over the time that has elapsed since the point  $(x, y)$  of the surface under consideration crossed this inlet boundary. For the steady-state problem considered here, the time integration becomes a spatial integration along the surface's path through the contact. The lowest Peclet number occurs in experiment 2-2, which has the slowest disc surface speeds—3.09 m/s for the slow disc. At the lowest load that was modelled (620 N), the contact semi-dimension,  $b$ , in the direction of sliding, is 0.29 mm. This gives a Peclet number of  $L = 35.6$  for this surface. Johnson [21] states that, for  $L > 5$ , the heat will only diffuse a short distance into the solid in the time taken for it to travel through the contact, and hence, the heat flow will be approximately perpendicular to the surface. Thus, the assumption of a one-dimensional conduction model is valid for the conditions considered in this work. This is confirmed by comparing with a model recently developed by the authors that includes a complete thermal analysis of the solids for the case with the smallest Peclet number.

#### 3.2 Solution method

The EHL solution method used in this study is presented in detail in references [12], [13], and [19] with equations (1) and (3) discretized using central differences with second-order accuracy. A flow diagram of the solution method is given in Fig. 4.

The solution to the thermal problem is achieved by solving equations (4) and (5) periodically during the overall EHL solution procedure. This is carried out in cycles of the main loop of the solver, which are specified as thermal correction cycles. Their frequency is varied so that the temperature distribution within the film becomes established as the EHL solution to equations (1) and (3) is obtained. Thus, the temperature dependence of viscosity is taken into account in determining the flow factors,  $\sigma_x$  and  $\sigma_y$ , in equation (1). In solving equation (4) numerically, the film is divided into  $n_f$  cross-film node points. The right-hand side, and the velocity- and pressure-gradient-dependent terms in  $\theta$  and its derivatives, is evaluated at each cross-film node point using the outer-loop values of these parameters. Second-order central difference expressions are used for the conductive derivative terms, whereas the appropriate backward or forward

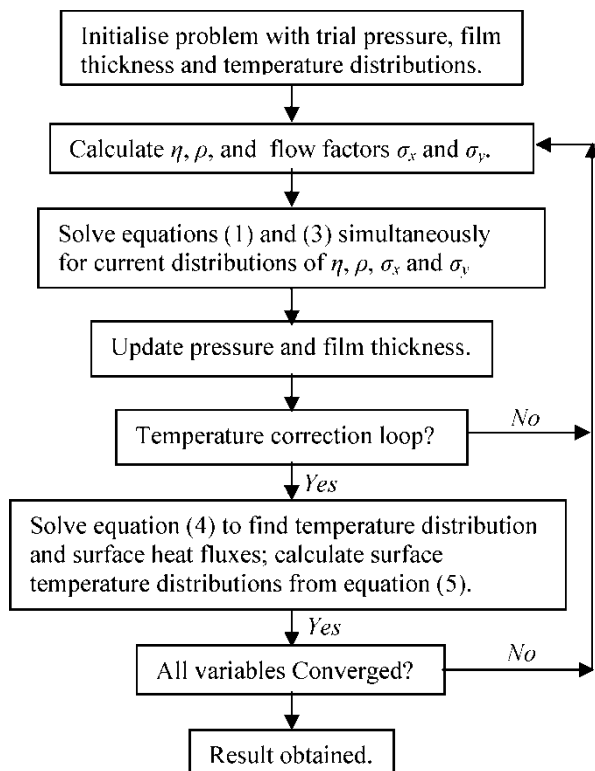


Fig. 4 Flow chart of the numerical solution procedure

difference expression is used for the convective terms depending on the sign of the fluid velocity components at each mesh point and cross-film level to achieve first-order upwind differencing. The current values of the surface temperatures are regarded as boundary conditions, and the remaining  $n_f - 2$  cross-film temperature values are obtained from the resulting tridiagonal system, using outer-loop temperature values at other  $(x, y)$  positions. The boundary conditions used for equation (4) for the oil film are that where the lubricant is flowing out of the solution area, the temperature gradient normal to the boundary is zero. Where the lubricant is flowing into the solution area, it does so at the surface temperature. These conditions are applied to each value of  $z$  according to the lubricant velocity components  $u(x, y, z)$  and  $v(x, y, z)$ .

The temperature gradient at each of the solid/liquid interfaces is then evaluated, to give the surface heat flux,  $q$ , so that equation (5) may be used to recalculate the surface temperatures. For each point on the surface, the integral of equation (5) is evaluated by transforming the time integral into a spatial integral, by taking note of the locus of the surface point in reaching its current position. It remains necessary to specify the surface temperature at the inlet to the EHL calculation region,  $\theta_B$ . This value is taken from the test disc and shaft heat transfer analysis described in section 2 and is the best estimate for the surface temperatures of the disc upstream of the contact area.

The thermal calculations are carried out periodically during the EHL convergence process. The interface temperature gradients and cross-film temperature field converge reliably and stabilize rapidly. The converged thermal EHL solution is obtained when the pressure, film thickness, and temperature fields converge, with the constant  $h_0$  in equation (2) adjusted to obtain the correct load.

### 3.3 Rheological models

In two-dimensional flow, as considered by the point contact model used in this work, the non-Newtonian formulation links shear stress to strain rate according to

$$\frac{\partial u}{\partial z} = \frac{\tau_x}{\tau_e} F(\tau_e), \quad \frac{\partial v}{\partial z} = \frac{\tau_y}{\tau_e} F(\tau_e) \quad (6)$$

where  $\tau_e = \sqrt{\tau_x^2 + \tau_y^2}$ . Two rheological models were included in the present study—the Eyring-type shear-thinning model as proposed by Johnson and Tevaarwerk [22] and the Bair and Winer model [23] that displays limiting shear stress behaviour. The forms used are shown in equations (7) and (8), respectively

$$F(\tau) = \frac{\tau_0}{\eta} \sinh\left(\frac{\tau}{\tau_0}\right) \quad (7)$$

$$F(\tau) = -\frac{\tau_L}{\eta} \ln\left(\frac{\tau_L - \tau}{\tau_L}\right) \quad (8)$$

The balance of forces on a fluid element ensures that the shear stress components vary linearly across the film

$$\tau_x(z) = \tau_{xm} + z \frac{\partial p}{\partial x}, \quad \tau_y(z) = \tau_{ym} + z \frac{\partial p}{\partial y} \quad (9)$$

Equation (6) may be integrated across the film, to give the difference between the velocity components at the solid/liquid boundaries. Thus, in the sliding ( $x$ ) and non-sliding ( $y$ ) directions, respectively

$$u_s = \int_{h/2}^{h/2} \frac{\tau_x}{\tau_e} F(\tau_e) dz \quad (10)$$

$$0 = \int_{h/2}^{h/2} \frac{\tau_y}{\tau_e} F(\tau_e) dz \quad (11)$$

where  $u_s$  is the sliding velocity. The values of the mid-film shear stress components  $\tau_{xm}$  and  $\tau_{ym}$  are determined, so that equations (10) and (11) are satisfied using a Newton method. The shear stresses in the energy equation are then known from equation (9) and the flow coefficients  $\sigma_x$  and  $\sigma_y$  in Reynolds equation are determined as described in reference [12].

### 3.4 Shear limit and slip

When a limiting shear stress rheological model, such as that given in equation (8), is used, the maximum shear stress that can develop in the film is constrained to not exceed the value of  $\tau_L$ , and thus, there is a maximum amount of sliding that the oil can provide,  $u_{Smax}$ . Equation (9) ensures that the largest value of  $\tau_e$  occurs at one or other of the fluid boundaries. When this occurs, the fluid experiences the largest possible amount of sliding that the limiting shear stress model can accommodate. The value of  $u_s$  is given by equation (10) for these circumstances. If  $u_s$  is greater than  $u_{Smax}$ , then the lubricant must compensate for this in some way. The oil is thus considered to slip, with slip velocity  $u_{slip} = u_s - u_{Smax}$ , along a slip plane which, in this study, has been taken to be at the point of highest temperature within the film. This is based on the observation that limiting shear stress levels generally fall with increasing temperature [24]. The power dissipated at the slip plane is  $\tau_x \cdot u_{slip}$ , and within the solution of the energy equation, this is added to the right-hand side of equation (4) at the cross-film node position corresponding to the slip plane.

When slip occurs in this way, the Couette component of the fluid flow is modified. This has the result that the entrainment velocity will vary between the surface velocities  $u_1$  and  $u_2$  according to the position of the slip plane. When slip occurs at the faster moving surface, the entrainment velocity is locally reduced to that of the slower moving surface, which has the effect of locally increasing the film thickness to maintain continuity. This is the case for the models described in this article for most of the area where slip is found to occur. In the exit to the contact where the pressure gradients are positive and extremely high, the highest shear stress occurs on the slower moving surface. The pressure gradients within the model can be such that  $(z/2)\sqrt{(\partial p/\partial x)^2 + (\partial p/\partial y)^2}$  is greater than the limiting shear stress. In those circumstances, the model used is that suggested by Ståhl and Jacobson [25] with slip at the slower surface, and it is found that this procedure leads to converged solutions where  $(z/2)\sqrt{(\partial p/\partial x)^2 + (\partial p/\partial y)^2}$  is below or equal to the limiting shear stress value. For the current work, the limiting shear stress is taken to be a function of pressure only. A more sophisticated approach where the limiting shear stress is also a specified function of temperature is under development.

### 3.5 Viscosity models

The present study investigates the use of three alternative models to determine the variation of viscosity with pressure and temperature, proposed by Bair [26], Roelands [27], and Barus.

The Bair formula

$$\eta = \eta_g \exp \left\{ \frac{-2.3C_1(T - T_g)F}{C_2 + (T - T_g)F} \right\} \quad (12)$$

where  $T_g = T_{g0} + A_1 \ln(1 + A_2 p)$  and  $F = 1 - B_1 \ln(1 + B_2 p)$  was used, with the parameters given by Bair [26] for a lubricant to specification Mil-L23699, to which the Mobil Jet 2 corresponds:  $\eta_g = 10^{12}$  Pa s,  $T_{g0} = -87^\circ\text{C}$ ,  $A_1 = 158^\circ\text{C}$ ,  $A_2 = 0.4476 \text{ GPa}^{-1}$ ,  $B_1 = 0.194 \text{ GPa}^{-1}$ ,  $B_2 = 18.8 \text{ GPa}^{-1}$ ,  $C_1 = 16.03^\circ\text{C}$ , and  $C_2 = 22.52^\circ\text{C}$ .

The Roelands expression was alternatively used

$$\eta = \eta_0 \exp \left\{ \ln \left( \frac{\eta_0}{\kappa} \right) \left[ (1 + \chi p)^Z \left( \frac{T + 135}{T_0 + 135} \right)^{-S_0} - 1 \right] \right\} \quad (13)$$

where  $\kappa = 63.15 \times 10^{-6}$  Pa s and  $\chi = 5.1 \text{ GPa}^{-1}$  were used to determine the variation of viscosity with pressure and temperature. Data from reference [28] were used to determine the ambient pressure-viscosity as

$$\eta_0 = 12.30 T_0^{-1.713} \text{ Pa s}$$

and the pressure-viscosity coefficient as

$$\alpha_0 = 60.36 T_0^{-0.3683} \text{ GPa}^{-1}$$

Parameter  $Z$  was obtained from the pressure-viscosity coefficient as  $Z = \alpha_0 / (\chi \ln(\eta_0/\kappa))$ . Parameter  $S_0$  was taken as 1.108 by fitting equation (15) of reference [29] to the viscosity data given in reference [28].

In addition, a Barus type viscosity formula was obtained, using the power law fits above for  $\eta_0$  and  $\alpha_0$  based on the data given in reference [28]

$$\eta = 12.30 T^{-1.713} \exp(60.36 \times 10^{-9} T^{-0.3683} p) \quad (14)$$

### 3.6 Lubricant conductivity

Larsson and Andersson [30] have reported transient hot-wire measurements of thermal conductivity, which show a doubling of the conductivity values over the range of pressures of interest in EHL modelling. One of the lubricants tested by Larsson and Andersson was a tri-methol-propynol ester, which is reasonably similar to the ester-based Mobil Jet 2, and they proposed the following model for the pressure dependence of thermal conductivity for this oil

$$k = 0.162 \left( 1 + \frac{1.44p}{1 + 0.56p} \right) \quad (15)$$

They also found that  $k$  had a minimal temperature dependence, which may be discounted for the range

of temperatures of interest in this study. Equation (15) was incorporated into the thermal EHL model as the best available estimate of the conductivity of the lubricant.

#### 4 RESULTS OF EHL MODELLING

In the present study, a steady-state thermal EHL solution was obtained for conditions at the end of each load stage in the experiments under consideration, where temperatures and friction force had reached approximately steady-state conditions. In order to investigate the influence of lubricant rheology on the thermal results (specifically the value of the heat partition parameter,  $\beta$ ), six different combinations of non-Newtonian model and viscosity model were used, as shown in Table 1. A solution was obtained using each of the six models shown in Table 1, at every load stage of each experiment. Details of the four experiments modelled, which used super-finished discs to eliminate any surface roughness effects, can be seen in Table 2. The experiments are numbered to be consistent with Patching [18] and Clarke [17]. The numerical resolution in the  $x$  and  $y$  axis directions in the contact plane was  $\Delta x = a/40$  and  $\Delta y = b/60$ . The cross-film resolution for the thermal calculations was  $n_f = 21$ , which was found by the authors to be sufficiently fine to give accurate solutions to the energy equation. A check calculation for one of the cases considered using  $n_f = 11$  gives the calculated  $\beta$  values that are within 2 per cent of those obtained with  $n_f = 21$ .

In order to match the calculated friction force to that recorded experimentally, the non-Newtonian parameter was adjusted until the calculated traction matched that recorded in the experiment. Data for these parameters for the temperatures and shear rates corresponding to the experiment are not known for the test lubricant, and it is clearly necessary that the energy dissipated in the modelled contact is the same as that measured in the disc test rig. In the case of the Johnson and Tevaarwerk model [22], the value of the Eyring stress,  $\tau_0$ , was assumed to be constant,

**Table 1** Models used in EHL analyses (numbers in brackets refer to the equations used)

Model	Rheology	Viscosity
A	Johnson and Tevaarwerk (7)	Bair (12)
B	Johnson and Tevaarwerk (7)	Roelands (13)
C	Johnson and Tevaarwerk (7)	Barus (14)
D	Bair and Winer (8)	Bair (12)
E	Bair and Winer (8)	Roelands (13)
F	Bair and Winer (8)	Barus (14)

whereas the limiting shear stress,  $\tau_L$ , in the Bair and Winer model [23], was assumed to vary proportionally with pressure (i.e.  $\tau_L = \gamma p$ ), with the value of the constant of proportionality being adjusted to match the recorded friction forces.

Once the model had converged, the heat flux into the solids was integrated over the surface area of each solid to calculate both the total heat passing into each surface and the value of the heat partition parameter,  $\beta$ .

As an example, results for the final load stage of experiment 2-13, where  $p_0 = 1.6$  GPa, are presented so as to compare the effects of the different rheological and viscosity models considered.

With Model A, which used the Eyring rheological model (equation (7)) together with the Bair viscosity (equation (12)), the correct friction force was obtained with the Eyring shear stress  $\tau_0 = 40$  MPa. This was sufficiently large to ensure that there was no significant non-Newtonian behaviour, as using the Bair viscosity data leads to essentially the correct friction force as measured in the experiment. The centre-line distributions of mid-film, fast- and slow-surface temperatures, and the heat fluxes on each surface can be seen in Fig. 5. It can be seen that both maximum surface temperatures are below the maximum mid-film oil temperature. Both surfaces attain similar maximum temperatures as they near the exit of the contact, yet the slow surface enters the contact at a temperature around 65 °C lower than the fast surface. The Newtonian behaviour in this EHL analysis leads to the shear heating being developed reasonably uniformly across the oil film. As can be seen from

**Table 2** Summary of scuffing tests

Test no.	2-2	2-5	2-11	2-13
Peripheral velocity of fast disk (m/s)	13.09	20.95	26.18	30.10
Peripheral velocity of slow disk (m/s)	3.09	4.95	6.17	7.10
Mean entraining velocity (m/s)	8.09	12.95	16.18	18.60
Sliding velocity (m/s)	10.00	16.00	20.00	23.00
Maximum recorded bulk temperature of fast disk (°C)	173	201	205	235
Maximum recorded bulk temperature of slow disk (°C)	130	153	152	170
Scuffing load (N)	3452	4150	3460	4160
Maximum Peak Hertzian contact pressure (GPa)	1.60	1.70	1.60	1.70
Mean frictional power intensity at scuffing load (MW/m <sup>2</sup> )	125.5	173.0	213.5	240.7

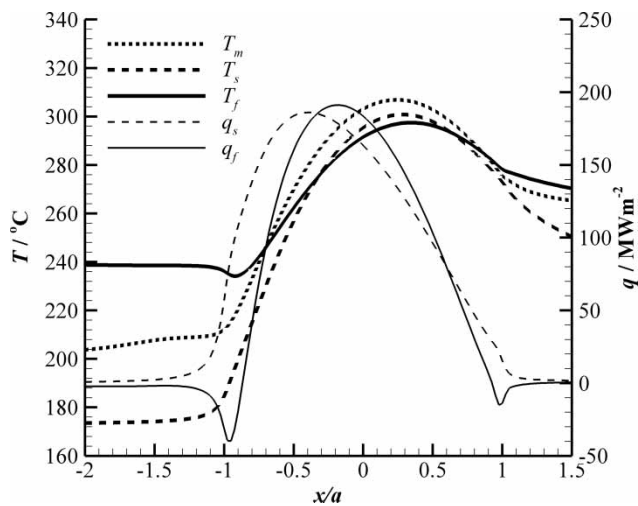


**Fig. 5** Centre-line mid-oil film and surface temperatures and surface heat fluxes, from EHL analysis using Model A

Fig. 5, the surface heat fluxes are of similar magnitude, and thus the slow surface, which spends more time in the contact, receives more heat energy and hence has a larger temperature rise when compared with the faster surface. The surface heat fluxes can be integrated over the contact area, allowing the heat partition parameter,  $\beta$ , to be calculated. For this case,  $\beta = 0.33$ , showing that the majority of the heat passes into the slower surface. This contrasts with the value of  $\beta$  calculated from the experimental data by the two-dimensional heat transfer modelling, where a value of  $\beta = 0.62$  was determined.

A further analysis was performed using Model B—i.e. the Eyring rheology with the Roelands viscosity model. Here,  $\tau_0 = 6.5$  MPa was required to match the predicted friction with the value recorded in the test. The value of  $\tau_e$  obtained in the results reached a level of 14.8 MPa, indicating that the non-Newtonian effects were active in the case considered. However, the results for this analysis showed little difference from those shown in Fig. 5.  $\beta$  was found to be 0.38, again favouring the slow surface.

Use of Model C, Eyring rheology with the Barus viscosity model, led to small differences in the temperatures and heat flux distributions, although they remain broadly similar to those of Fig. 5. The viscosity in the high-pressure region of the contact was considerably higher with the Barus model than with either of the other two viscosity formulas. As a result, the friction force generated under Newtonian conditions was higher and a significant degree of non-Newtonian behaviour was necessary to obtain the correct, experimentally measured, friction force. Using the Eyring model, a value of  $\tau_0 = 1.13$  MPa was found to give the measured friction. Again, the heat dissipated in this

model was relatively uniformly distributed across the film, with  $\beta = 0.37$ .

These three thermal EHL models gave  $\beta$  values in the range 0.33–0.38, which corresponds to most of the dissipated heat passing into the slower surface. The value of  $\beta$  determined from the two-dimensional heat transfer modelling [17] was 0.62, which corresponds to most of the dissipated heat passing into the faster surface. In an attempt to further explain this apparently contradictory behaviour of the thermal EHL analysis, a further three EHL simulations were performed using the Bair and Winer limiting shear stress rheological model. The results of Model D, which uses the limiting shear stress rheology with the Bair viscosity, were again very similar to those of Fig. 5. As in the case of Model A, the correct friction as measured in the experiment was obtained with essentially Newtonian behaviour, as the  $\tau_L$  value required was  $0.10p$ . Again, the slow surface experienced a larger temperature rise in the contact and the surface heat fluxes were of similar magnitude. This model gave a heat partition of  $\beta = 0.34$ .

The results of Model E, using the limiting shear stress rheology but with the Roelands viscosity model, were again very similar to Model D, with  $\beta = 0.37$ . However, the non-Newtonian behaviour with  $\tau_L = 0.0168p$  was necessary to achieve the correct friction force.

The results of Models A to E are generally similar to those shown in Fig. 5 and the values of maximum temperatures and maximum heat fluxes are given in Table 3.

Finally, an EHL simulation using Model F, with limiting shear stress rheology together with the higher Barus viscosity model, was carried out. The sliding demand made of the oil at this load was such that  $u_s$  exceeded  $u_{smax}$  over most of the Hertzian area. Hence, slip occurred within the fluid and is taken to occur where the temperature was highest across the film, as explained in section 3.4. This was found to be at, or near to, the faster surface. The thermal analysis uses 21 cross-film mesh points at each tangent plane mesh position. The energy dissipated at the slip plane was added to the lubricant at a single mesh point. This

**Table 3** Comparison of maximum temperature and maximum heat flux values obtained in analysing the test case (test 2-13,  $p_0 = 1.6$  GPa) with Models A to F

Model	$T_{om}$ (°C)	$T_{fm}$ (°C)	$T_{sm}$ (°C)	$q_{fm}$ (MW/m <sup>2</sup> )	$q_{sm}$ (MW/m <sup>2</sup> )
A	307	297	300	191	186
B	314	296	300	162	170
C	311	300	305	170	162
D	308	298	302	194	188
E	312	303	307	196	184
F	297	324	262	229	102

means that the slip energy is dissipated over 5 per cent of the film thickness. The results of this calculation can be seen in Fig. 6. The faster surface remains at a higher temperature than the slower surface throughout the contact. The maximum temperature within the film is also shown in Fig. 6 – this occurs at or close to the faster surface and exceeds the faster surface temperature by not more than 9°C for the case presented here.

Some 93 per cent of the energy is dissipated at the slip surface. Thus, the heat generated within the contact is concentrated near the fast surface, and the heat that reaches the slow surface has to be transmitted by conduction across the oil film. This leads to the heat partition favouring the faster surface, with  $\beta = 0.57$ , which is in much better agreement with the value  $\beta = 0.62$  obtained previously from the heat transfer analysis. The surface temperature behaviour is markedly different in this case. The difference between the surface temperatures is more or less maintained with the faster surface temperature being at least 60°C higher than the slower surface throughout. The oil mid-plane temperature is seen to be intermediate, which is expected as the oil is now primarily conducting heat across the film from the high-temperature surface to the low-temperature surface and its energy dissipation role is much reduced. An additional temperature trace corresponding to the maximum film temperature is included in Fig. 6 and the maximum temperature and heat flux values for the model are also given in Table 3. The different temperature behaviour of Model F is further illustrated by comparing Figs 7(a) and (b), which show the cross-film centre-line temperature distribution for Models A and

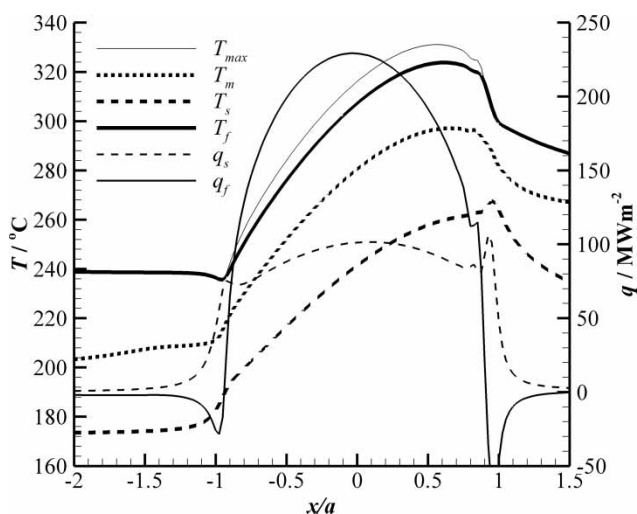


**Fig. 6** Centre-line mid-oil film and surface temperatures and surface heat fluxes, from EHL analysis using Model F

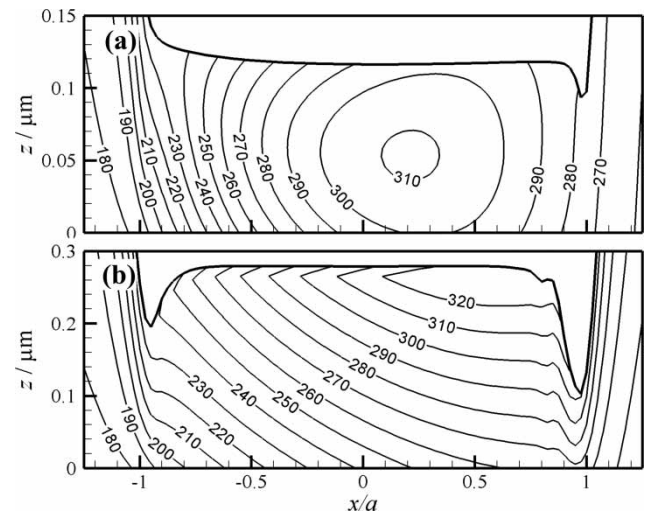


**Fig. 7** Cross-film oil temperature profiles at the plane  $y = 0$  (a) for Model A and (b) for Model F

F, respectively. The temperature contours in Fig. 7(a) are typical of the results of Models A–E, where shear heating is reasonably evenly distributed across the film. This leads to the maximum temperature being developed approximately at the mid-film position, with temperatures decreasing towards both surfaces. Figure 7(b), however, shows a significantly different temperature distribution, as the majority of the shear is concentrated near the fast surface. The maximum temperature occurs very near to the faster surface at the slip plane, and the temperature decreases towards the slow surface, as heat is conducted from the slip plane across the film. The effect of slip at the faster surface in reducing the entrainment velocity is seen in the changed film thickness developed over the slip region. This increase in film thickness increases the  $\beta$ -value by reducing the amount of heat conducted across the film.

The six different models were run for each load stage of the four experiments modelled, and the heat partition results obtained are shown in Table 4. It can be seen that, for all the experiments modelled, only Model F (limiting shear stress and Barus viscosity) was able to approach the heat partition calculated using the two-dimensional heat transfer modelling. This is further illustrated by Figs 8 and 9, which show the heat partition results for each test modelled. The solid line denoted 'Experiment' is the trend line fitted to the  $\beta$  values calculated using the heat transfer modelling described in reference [17], as shown in Fig. 3. The points in Fig. 8 are the  $\beta$ -values calculated using EHL Models A to E described above. Although there are differences between the results produced by each of the models illustrated in Fig. 8, they are in general agreement, predicting that a maximum of 55 per cent of the heat passes into the fast disc at low values of  $\Delta Tu_s$

**Table 4** Summary of  $\beta$ -values

Test no.	$p_0$ (Gpa)	$\beta$ - values from two-dimensional conduction model [13]	Value of heat partition parameter, $\beta$ , calculated from thermal EHL models					
			A	B	C	D	E	F
2-2	1.0	0.740	0.509	0.510	0.514	0.510	0.512	0.716
	1.1	0.720	0.488	0.487	0.487	0.486	0.486	0.664
	1.2	0.700	0.470	0.467	0.456	0.458	0.458	0.662
	1.3	0.670	0.445	0.445	0.433	0.436	0.435	0.615
	1.4	0.660	0.423	0.431	0.440	0.436	0.442	0.587
	1.5	0.650	0.401	0.414	0.420	0.424	0.434	0.557
2-5	1.1	0.690	0.488	0.487	0.494	0.498	0.494	0.739
	1.2	0.690	0.476	0.474	0.479	0.477	0.478	0.713
	1.3	0.670	0.467	0.465	0.468	0.469	0.468	0.685
	1.4	0.670	0.449	0.442	0.445	0.450	0.450	0.646
	1.5	0.650	0.440	0.438	0.441	0.443	0.443	0.627
	1.6	0.630	0.429	0.436	0.439	0.437	0.442	0.608
	1.7	0.620	0.402	0.423	0.429	0.410	0.432	0.579
2-11	0.9	0.790	0.487	0.487	0.509	0.490	0.490	0.653
	1.0	0.720	0.481	0.482	0.494	0.484	0.485	0.765
	1.1	0.700	0.472	0.474	0.480	0.478	0.477	0.743
	1.2	0.670	0.463	0.469	0.472	0.468	0.472	0.722
	1.3	0.650	0.455	0.466	0.468	0.460	0.466	0.700
	1.4	0.640	0.430	0.444	0.445	0.437	0.450	0.659
	1.5	0.630	0.397	0.423	0.426	0.404	0.432	0.621
1.6	0.630	0.339	0.391	0.396	0.348	0.403	0.572	
2-13	0.9	0.730	0.526	0.515	0.546	0.565	0.561	0.712
	1.0	0.730	0.504	0.493	0.532	0.563	0.552	0.751
	1.1	0.700	0.480	0.477	0.503	0.498	0.531	0.729
	1.2	0.670	0.462	0.462	0.460	0.470	0.470	0.707
	1.3	0.640	0.453	0.454	0.450	0.453	0.454	0.691
	1.4	0.630	0.429	0.433	0.425	0.428	0.427	0.659
	1.5	0.630	0.385	0.405	0.392	0.388	0.394	0.609
	1.6	0.620	0.330	0.383	0.371	0.340	0.371	0.571

with the proportion falling to as little as 33 per cent for the higher values of  $\Delta Tu_s$ . These trends are markedly different from those of the experimentally obtained  $\beta$ -values that range between 75 and 63 per cent.

The results shown in Fig. 9 are those obtained with Model F and all showed slip at or near the faster fluid–solid boundary, with typically some 90 per cent or more of the heat being dissipated at the slip plane.

At the lowest load stage of test 2-13, a smaller level of slip was required with some 58 per cent of the heat dissipated at the slip plane. For the other cases, over 90 per cent was dissipated at the slip plane. This explains why the  $\beta$ -value for the lowest load point does not follow the trend of the remaining points from test 2-13. This model is much more successful in predicting the experimentally measured heat partition. The results

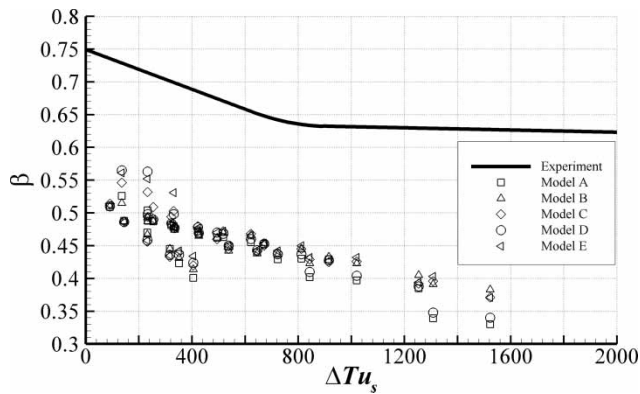


**Fig. 8** Comparison of heat partition parameter,  $\beta$ , calculated by EHL analysis (data points) with  $\beta$ -values calculated from experimental data (solid line) using Models A–E

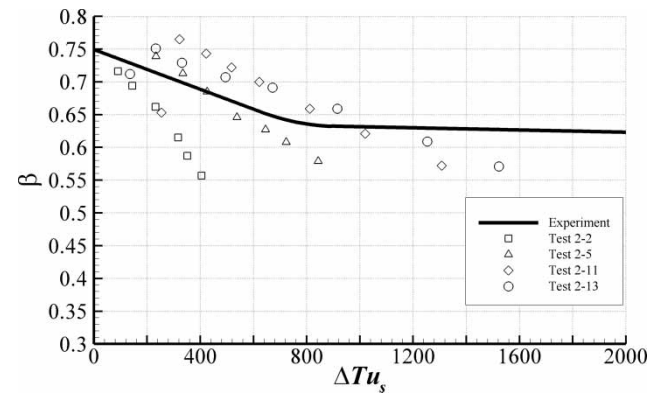


**Fig. 9** Comparison of heat partition parameter,  $\beta$ , calculated by EHL analysis (data points) with  $\beta$ -values calculated from experimental data (solid line) using Model F

do not follow the experimental trend in a detailed way, but are at the correct level with differences in detail. This is in marked contrast to Fig. 8, which shows results that are consistent with each other but in significant conflict with the experimentally determined  $\beta$ -values. It is clear that only when the limiting shear stress rheology is used with the Barus viscosity law are heat partition results obtained which approach those determined through heat transfer modelling of the disc machine experiments.

## 5 DISCUSSION AND CONCLUSIONS

The results presented suggest that the thermal EHL model with the best available viscosity data does not predict the correct heat partition, as calculated from the previous heat transfer analysis of the discs. Four experiments have been modelled, which have a total of 29 different load stages, each of which has been analysed using the thermal EHL solver with six different combinations of rheological and viscosity model. The results from these analyses follow a consistent trend: only when the higher Barus viscosity is used in conjunction with a limiting shear stress rheological model, which ensures that lubricant slip takes place, do the heat partition results favour the faster disc.

It remains to be seen whether this discrepancy is due to inaccuracies in the thermal EHL model, inaccuracies in the heat transfer modelling of the discs, or discrepancies in the way in which the viscosity is specified. However, the conclusion that more heat passes into the faster disc is consistent with the previous disc machine work by Merritt [31], for example.

The potential uncertainties in the heat transfer analysis stem from the assumed heat transfer coefficients used in the model. These are discussed in detail in reference [17], and the authors are currently developing more highly instrumented disc machines that will allow new experiments and further modelling work to be carried out to higher precision and with all uncertainties relating to heat transfer coefficients eliminated. Although the results obtained for  $\beta$  with Model F are much closer to the values deduced from the experiments, they do not show the levelling off with increasing  $\Delta Tu_s$  seen in Fig. 4. One possible explanation is that this feature is caused by changes to the experimental discs' heat transfer characteristics caused by relative surface temperature and relative speed in the enclosed environment of the test head. The planned experiments with distributed temperature measurement will only require one heat transfer coefficient to be obtained. It will be then possible to deduce this value experimentally for each rig operating condition.

Conclusions that can be drawn from this work are as follows.

1. Extensive EHL modelling using currently available rheological and viscosity models has shown significant contradictions with heat partition behaviour previously deduced from experiments.
2. In order to reproduce similar heat partition to that measured experimentally, it is necessary to use a limiting shear stress rheological model together with the higher Barus viscosity. This gives slip within the film, which occurs at or near the faster surface. Therefore, the distribution of shear heating across the film is not even, with high shear concentrated close to the faster surface. Such a shear distribution is necessary to reproduce the heat partition deduced from the experiments.
3. The combination of the thermal EHL modelling reported here and a suitably instrumented disc machine with detailed heat partition analysis offers considerable promise as a means of studying the rheological and traction behaviour of lubricants in an EHL contact. This has the potential to become a much more discerning experimental technique for comparing EHL rheological models than the conventional approach of simple friction measurement in EHL contacts.

## ACKNOWLEDGEMENTS

The authors gratefully acknowledge the support of EPSRC award GR/T05059 to the research project of which this investigation forms a part and of Shell Global Solutions for their contribution to the studentship of the first author. They would also like to thank Dr P Verne for his helpful comments on the original manuscript that led the authors to develop the limited shear stress model results in the form presented in the paper.

## REFERENCES

- 1 **Blok, H.** Theoretical study of temperature rise of surfaces of actual contact under oiliness lubricating conditions. In *Proceedings of General Discussion on Lubrication*, part 2, 1937, pp. 222–235 (Institution of Mechanical Engineers, London).
- 2 **Blok, H.** The constancy of scoring temperature. In *Interdisciplinary approach to the lubrication of concentrated contacts*. NASA Special Publication SP237, 1969 (NASA, New York).
- 3 **Tian, X. and Kennedy, F. E.** Maximum and average flash temperatures in sliding contacts. *Trans. ASME, J. Tribol.*, 1994, **116**, 167–174.
- 4 **Bos, J. and Moes, H.** Frictional heating of tribological contacts. *Trans. ASME, J. Tribol.*, 1995, **117**, 171–177.

- 5 Manton, S. M., O'Donoghue, J. P., and Cameron, A. Temperatures at lubricated rolling/sliding contacts. *Proc. Instn Mech. Engrs*, 1967, **182**, 813–823.
- 6 Cheng, H. S. A refined solution to the thermal elastohydrodynamic lubrication of rolling and sliding cylinders. *Trans. ASLE*, 1965, **8**, 397–410.
- 7 Sadeghi, F. and Sui, P. C. Thermal elastohydrodynamic lubrication of rolling/sliding contacts. *Trans. ASME, J. Tribol.*, 1990, **112**, 189–195.
- 8 Sui, P. C. and Sadeghi, F. Non-Newtonian thermal elastohydrodynamic lubrication. *Trans. ASME, J. Tribol.*, 1991, **113**, 390–397.
- 9 Yang, P. and Wen, S. A generalized Reynolds equation for non-Newtonian thermal elastohydrodynamic lubrication. *Trans. ASME, J. Tribol.*, 1990, **112**, 631–636.
- 10 Hsiao, H.-S. H. and Hamrock, B. J. Temperature distribution and thermal degradation of the lubricant in EHL line contact conjunctions. *Trans. ASME, J. Tribol.*, 1994, **116**, 794–803.
- 11 Wolff, R., Nonaka, T., Kubo, A., and Matsuo, K. Thermal elastohydrodynamic lubrication of rolling/sliding line contacts. *Trans. ASME, J. Tribol.*, 1992, **114**, 706–713.
- 12 Sharif, K. J., Kong, S., Evans, H. P., and Snidle, R. W. Contact and elastohydrodynamic analysis of worm gears – Part 1: theoretical formulation. *Proc. Instn Mech. Engrs, Part C: J. Mechanical Engineering Science*, 2001, **215**, 817–830.
- 13 Sharif, K. J., Evans, H. P., Snidle, R. W., and Newall, J. P. Modelling of film thickness and traction in a variable ratio traction drive rig. *Trans. ASME, J. Tribol.*, 2004, **126**, 92–104.
- 14 Yang, P., Wang, J., and Kaneta, M. Thermal and non-Newtonian numerical analyses for starved EHL line contacts. *Trans. ASME, J. Tribol.*, 2006, **128**, 282–290.
- 15 Chang, L. Traction in thermal elastohydrodynamic lubrication of rough surfaces. *Trans. ASME, J. Tribol.*, 1992, **114**, 186–191.
- 16 Zhu, D. and Hu, Y.-Z. A computer program package for the prediction of EHL and mixed lubrication characteristics, friction, subsurface stresses and flash temperatures based on measured 3-D surface roughness. *Tribol. Trans.*, 2001, **44**, 383–390.
- 17 Clarke, A., Sharif, K. J., Evans, H. P., and Snidle, R. W. Heat partition in rolling/sliding elastohydrodynamic contacts. *Trans. ASME, J. Tribol.*, 2006, **128**, 67–84.
- 18 Patching, M. J., Kweh, C. C., Evans, H. P., and Snidle, R. W. Conditions for scuffing failure of ground and superfinished steel discs at high sliding speeds using a gas turbine engine oil. *Trans. ASME, J. Tribol.*, 1995, **117**, 482–489.
- 19 Holmes, M. J. A., Evans, H. P., Hughes, T. G., and Snidle, R. W. Transient elastohydrodynamic point contact analysis using a new coupled differential deflection method: part 1 theory and validation. *Proc. Instn Mech. Engrs, Part J: J. Engineering Tribology*, 2003, **217**, 289–303.
- 20 Evans, H. P. and Hughes, T. G. Evaluation of deflection in semi-infinite bodies by a differential method. *Proc. Instn Mech. Engrs, Part C: J. Mechanical Engineering Science*, 2000, **214**, 563–584.
- 21 Johnson, K. L. *Contact mechanics*, 1985 (Cambridge University Press, Cambridge).
- 22 Johnson, K. L. and Tevaarwerk, J. L. Shear behaviour of elastohydrodynamic oil films. *Proc. R. Soc. Lond. A*, 1977, **356**, 215–236.
- 23 Bair, S. and Winer, W. O. A rheological model for elastohydrodynamic contacts based on primary laboratory data. *Trans. ASME, J. Lubr. Technol.*, 1979, **101**, 258–265.
- 24 Bair, S. and Winer, W. O. Shear strength measurements of lubricants at high pressure. *Trans. ASME, J. Lubr. Technol.*, 1979, **101**, 251–257.
- 25 Ståhl, J. and Jacobson, B. O. A lubricant model considering wall-slip in EHL line contacts. *Trans. ASME, J. Tribol.*, 2003, **125**, 523–532.
- 26 Bair, S. The variation of viscosity with temperature and pressure for various real lubricants. *Trans. ASME, J. Tribol.*, 2001, **123**, 433–436.
- 27 Roelands, C. J. A. *Correlation aspects of the viscosity-temperature-pressure relationship of lubricating oils*. PhD Thesis, Technical University Delft, The Netherlands, 1966 (V.R.B. Gronigen, The Netherlands).
- 28 *Mobil EHL Guide Book*, 1979 (Mobil Oil Corporation, Products Department, New York).
- 29 Larsson, R., Larsson, P. O., Eriksson, E., Sjöberg, M., and Höglund, E. Lubricant properties for input to hydrodynamic and elastohydrodynamic lubrication analyses. *Proc. Instn Mech. Engrs, Part J: J. Engineering Tribology*, 2000, **214**, 17–28.
- 30 Larsson, R. and Andersson, O. Lubricant thermal conductivity and heat capacity under high pressure. *Proc. Instn Mech. Engrs, Part J: J. Engineering Tribology*, 2000, **214**, 337–342.
- 31 Merritt, H. E. Gear tooth contact phenomena. *Proc. Instn Mech. Engrs*, 1962, **176**, 141–154.

## APPENDIX

### Notation

$c$	specific heat capacity (J/kg K)
$E'$	effective modulus of elasticity (Pa)
$f_{i,j}$	pressure coefficient in the differential deflection equation ( $m^{-1}$ )
$h$	film thickness (m)
$h_0$	constant in the film thickness equation (m)
$k$	thermal conductivity (W/m K)
$L$	Peclet number
$p$	pressure (Pa)
$q_{fm}$	maximum fast surface heat flux ( $W/m^2$ )
$q_{sm}$	maximum slow surface heat flux ( $W/m^2$ )
$R$	radius of relative curvature (m)
$T_{fm}$	maximum temperature on the fast surface ( $^{\circ}C$ )
$T_{om}$	maximum mid-film oil temperature ( $^{\circ}C$ )
$T_{sm}$	maximum temperature on the slow surface ( $^{\circ}C$ )
$\hat{u}$	mean surface velocity in the $x$ direction (m/s)
$u_s$	sliding velocity (m/s)

---

$u, v$	velocities in the $x$ and $y$ directions (m/s)	$\eta_0$	ambient viscosity (Pa s)
$x, y$	coordinates in the contact plane (m)	$\theta$	temperature (K)
$z$	coordinate normal to the contact plane (m)	$\rho$	density (kg/m <sup>3</sup> )
		$\sigma_x, \sigma_y$	flow factors in axis directions (m s)
$\alpha_0$	pressure–viscosity coefficient (Pa <sup>-1</sup> )	$\tau$	shear stress (Pa)
$\beta$	heat partition parameter	$\tau_0$	Eyring shear stress (Pa)
$\eta$	viscosity (Pa s)	$\tau_L$	limiting shear stress (Pa)